Substituents drive ligand rearrangements, giving dinuclear rather than mononuclear complexes, and tune $Co^{II/III}$ redox potential

Fabrice N. H. Karabulut, Humphrey L. C. Feltham and Sally Brooker*

Department of Chemistry, University of Otago, PO Box 56, Dunedin 9054, New Zealand

CORRECTED

Electronic Supplementary Information

Literature of analogues of N,N’-bis(2-pyridylmethyl)di-[amine/imine] type ligand including hexa-, penta- and tetra-dentate

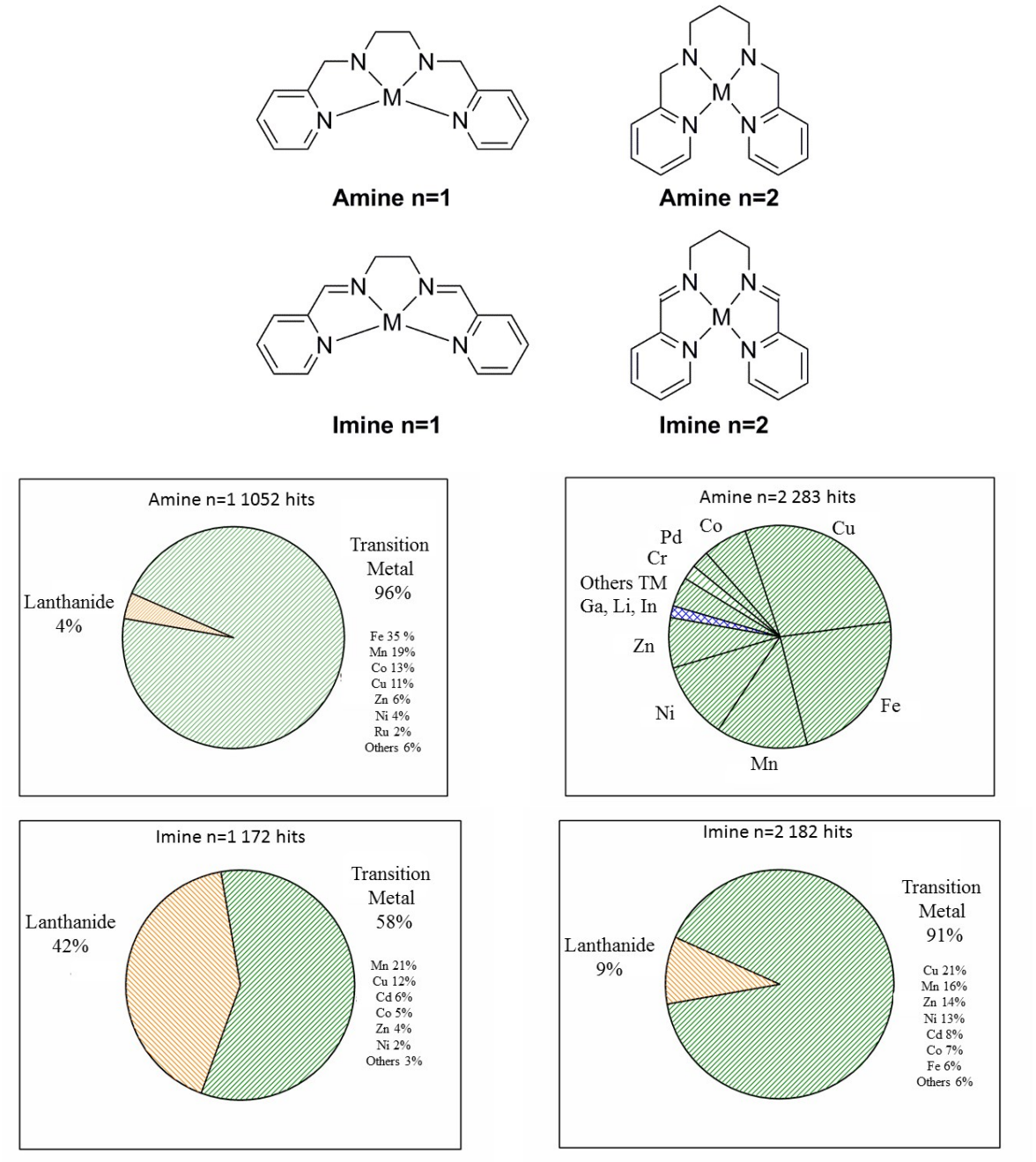

Figure S1. Results of CSD database searches (CSD version 5.39 November 2017) for all complexes of Schiff base N,N’-bis(2-pyridylethyl)di-[imine/amine] type ligands. Transition metals in green shading; lanthanides in orange shading; other metals in blue shading. (Amine or imine and n = 1 or 2 search fragments used for each of these are shown above).

NMR spectra

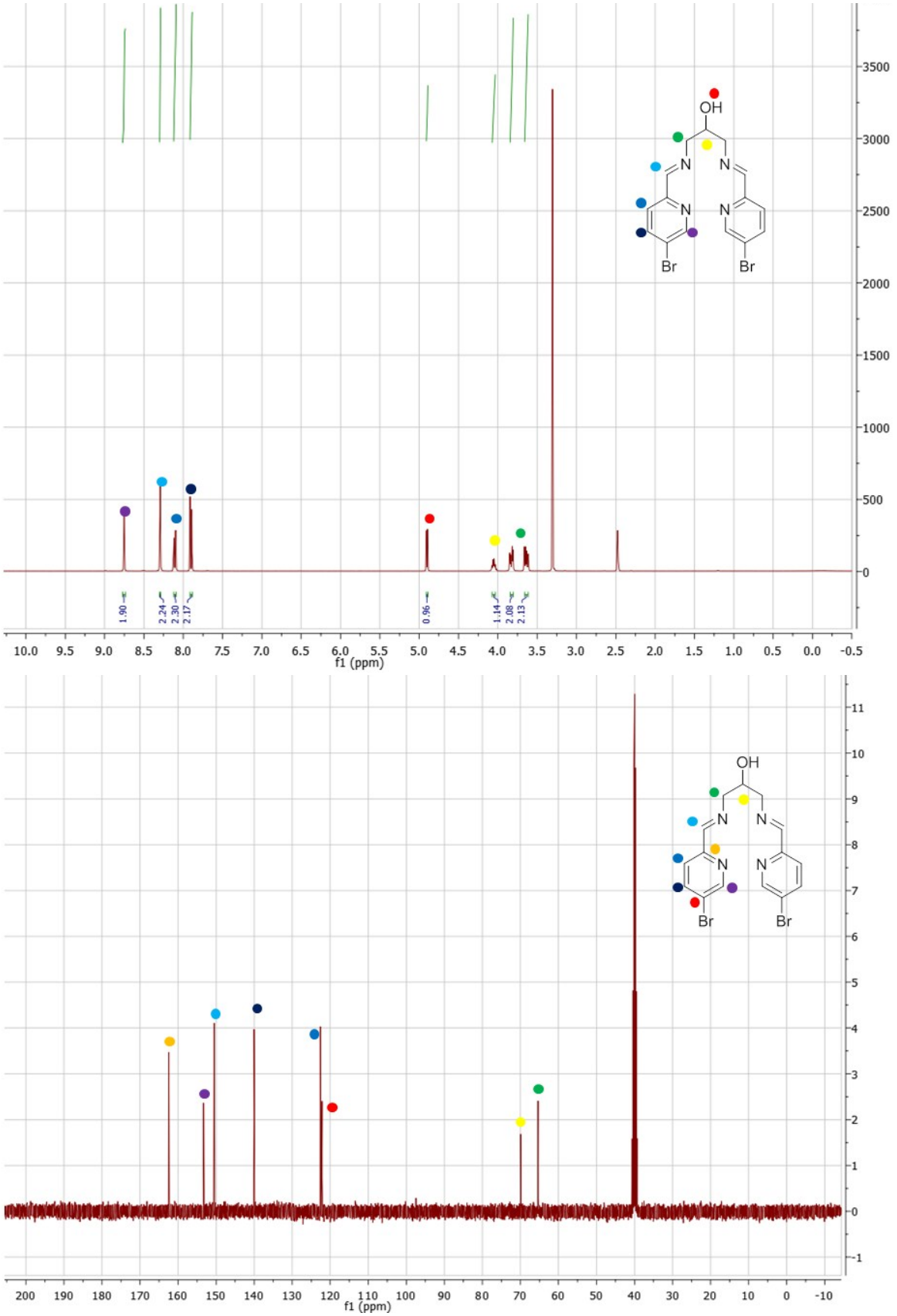

Figure S2. ^{1}H and ^{13}C NMR spectra of HL^{HBr} in DMSO at 298K (^{1}H: 400MHz, ^{13}C: 100MHz)

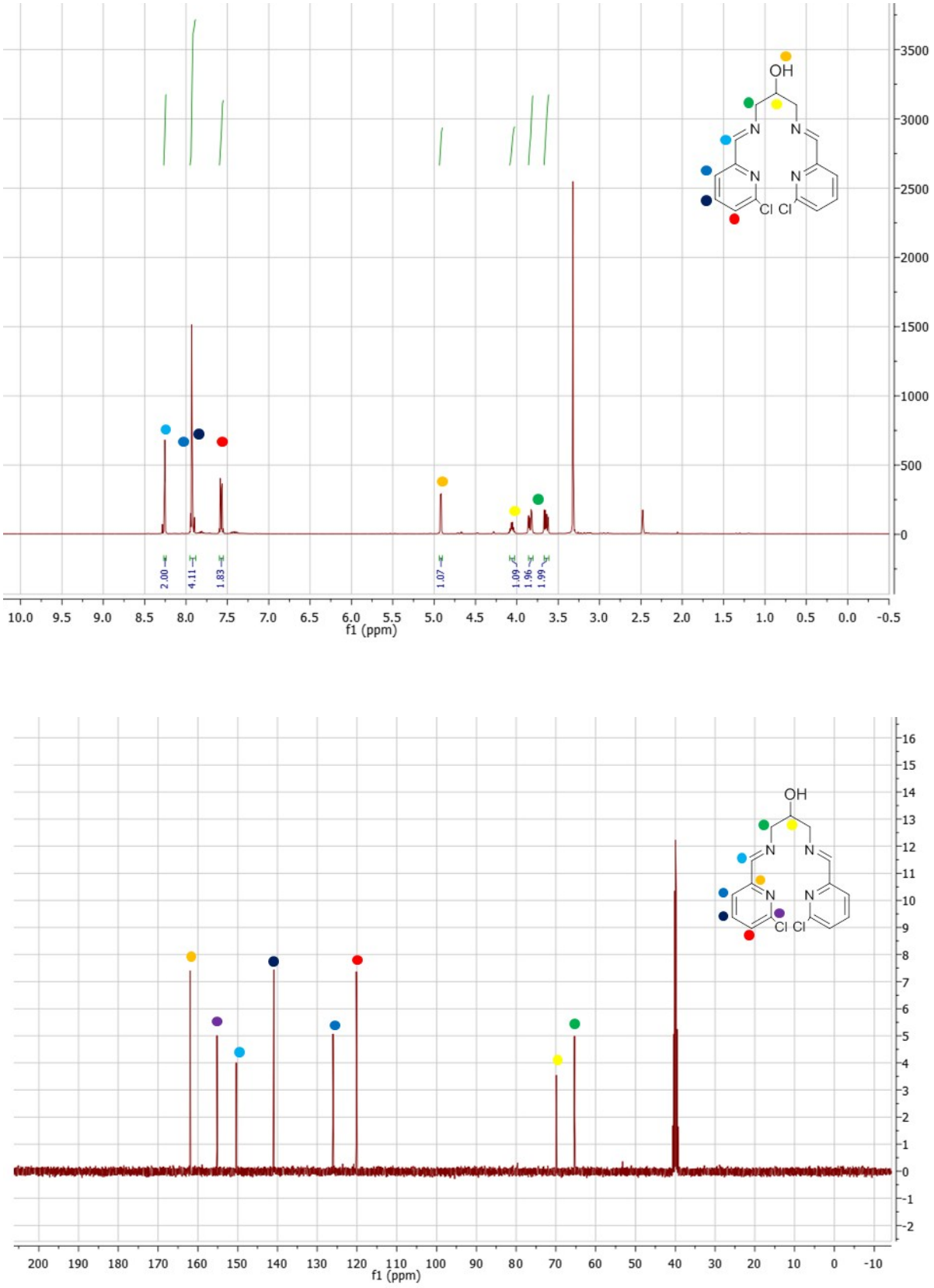

Figure S3. ^{1}H and ^{13}C NMR spectra of HL^{ClH} in DMSO at 298K (^{1}H: 400MHz, ^{13}C: 100MHz)

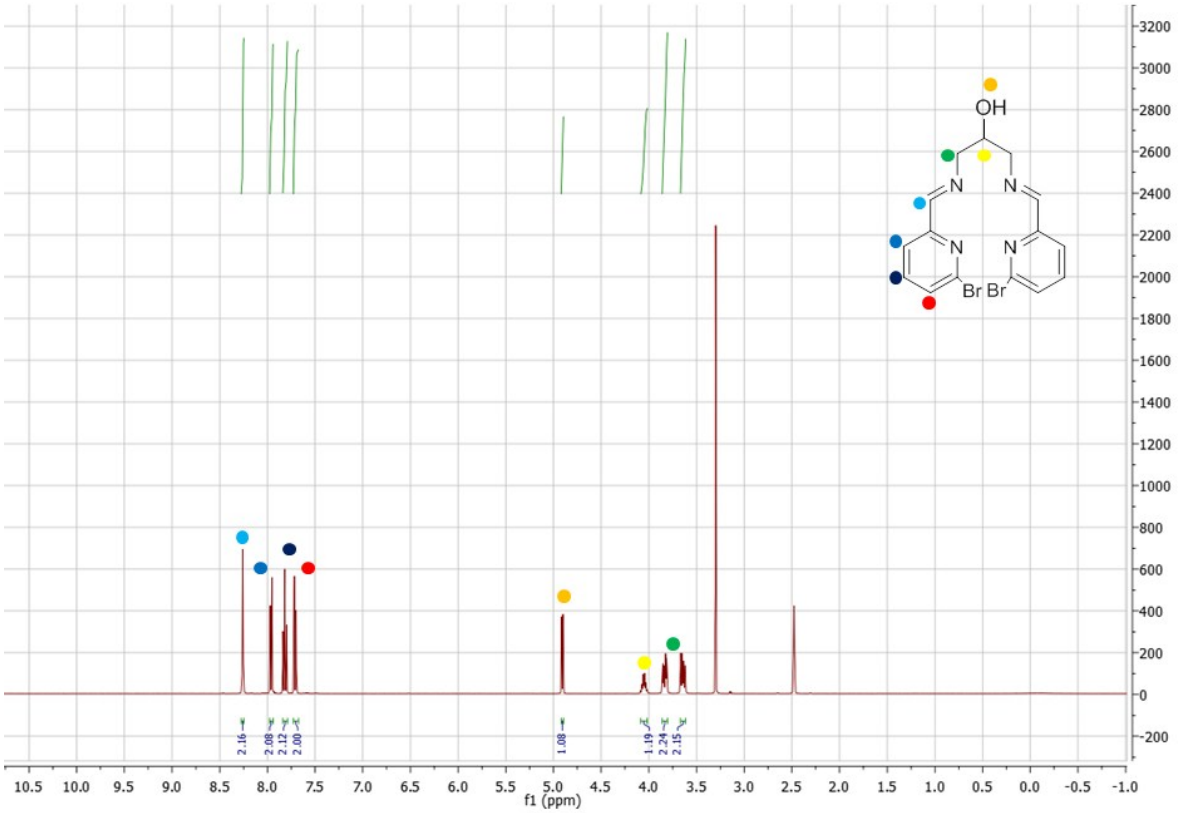

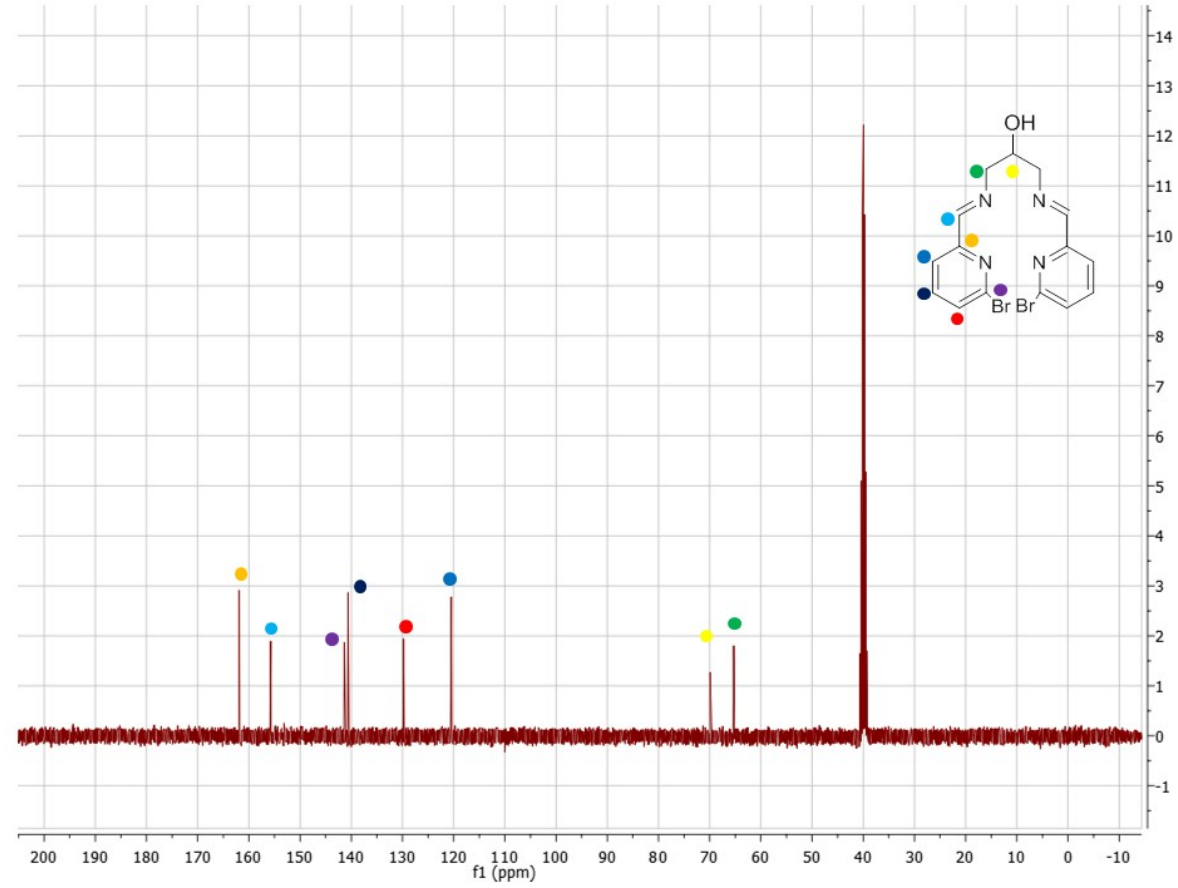

Figure S4. ^{1}H and ^{13}C NMR spectra of HL^{BrH} in DMSO at 298K (^{1}H: 400MH, ^{13}C: 100MHz)

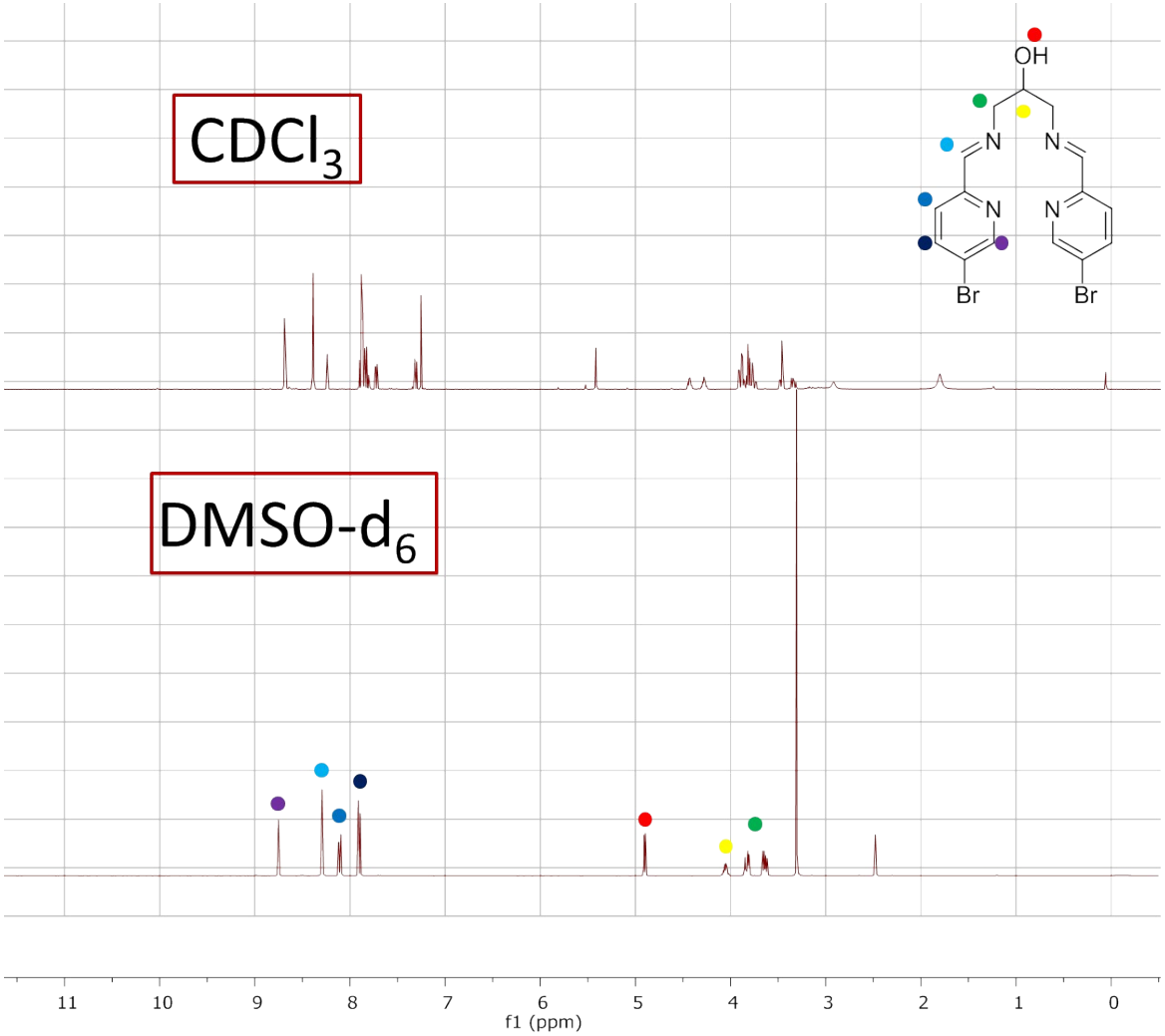

Figure S5. Stack plot of ^{1}H NMR spectra of H**L**$^{\mathbf{HBr}}$ in DMSO-d_6 versus $CDCl_3$

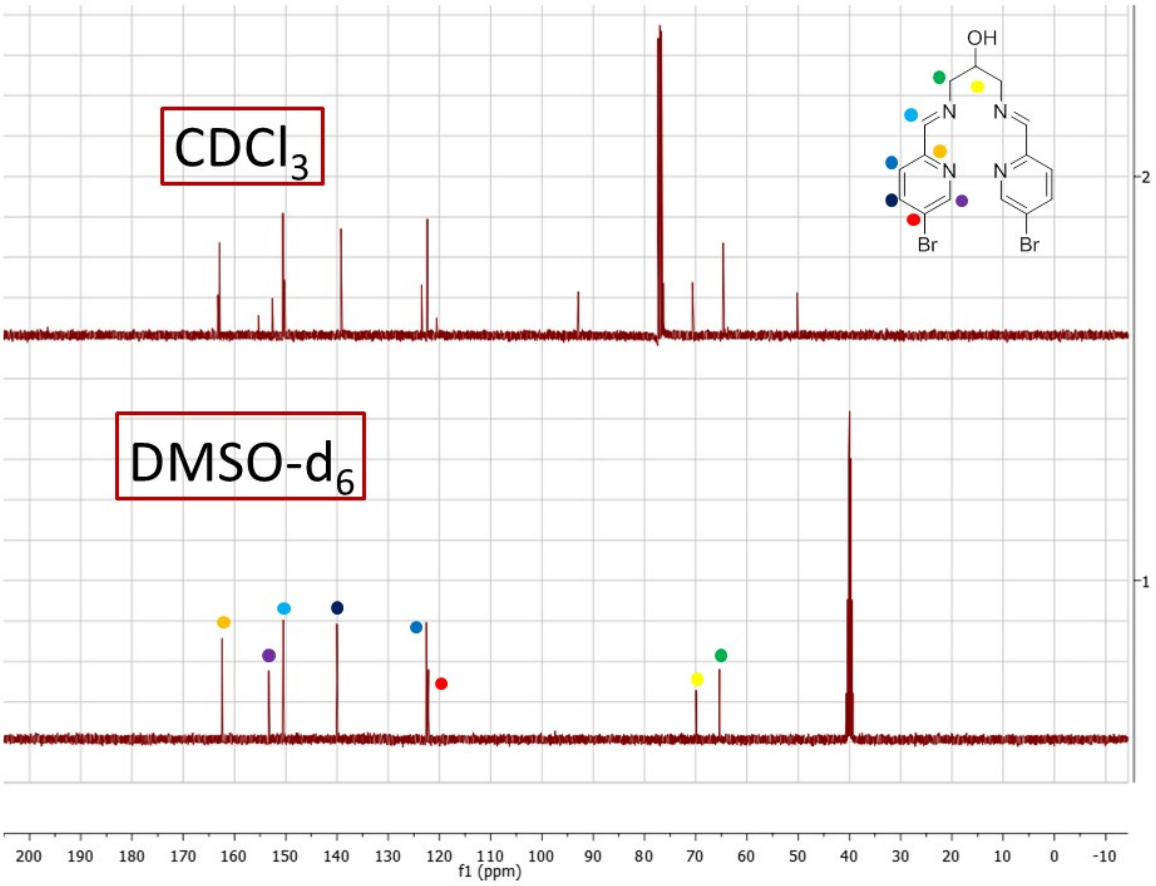

Figure S6. Stack plot of ^{13}C NMR spectra of H**L**^{HBr} in DMSO-d_6 versus $CDCl_3$

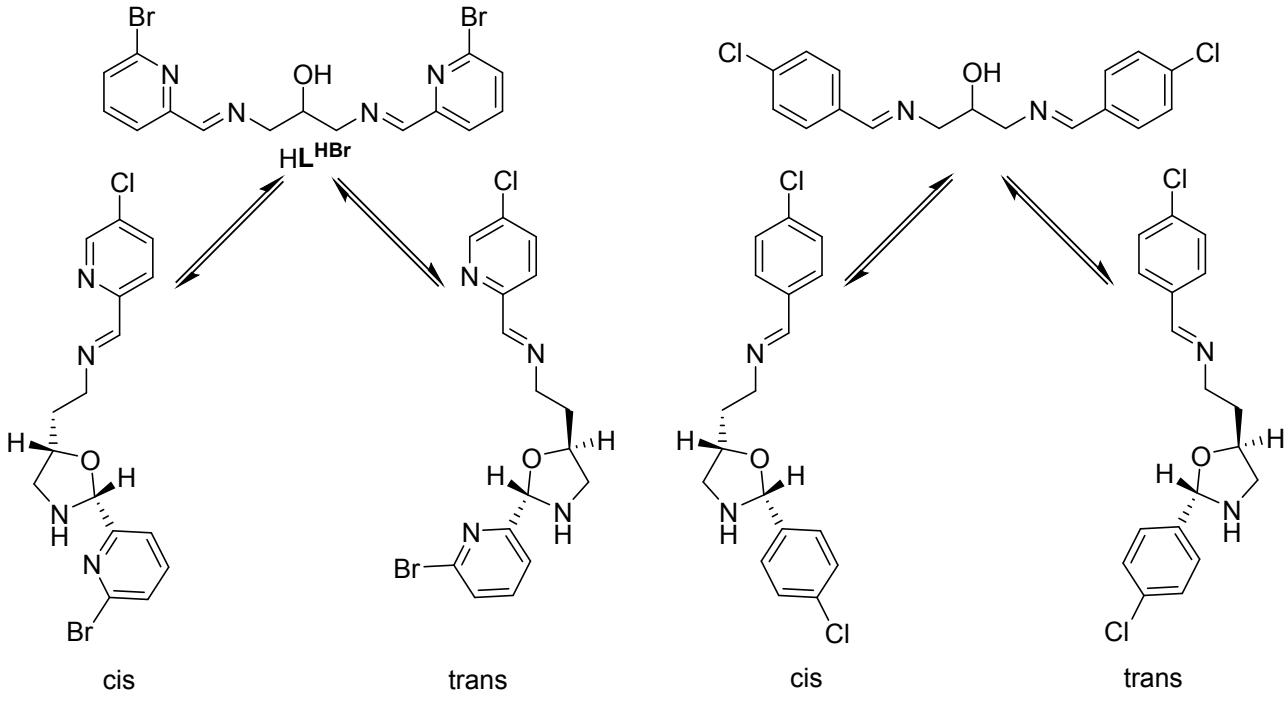

Figure S7. Possible ring-chain tautomeric equilibrium of: (left) compound H**L**^{HBr} in $CDCl_3$ solvent, which is not observed in DMSO-d_6 (see Figures S4 and S5), and (right) an analogous system studied by Crumbie etc.[1]

Comparison of IR spectra of mono- and di-nuclear cobalt(II) BF_4 complexes

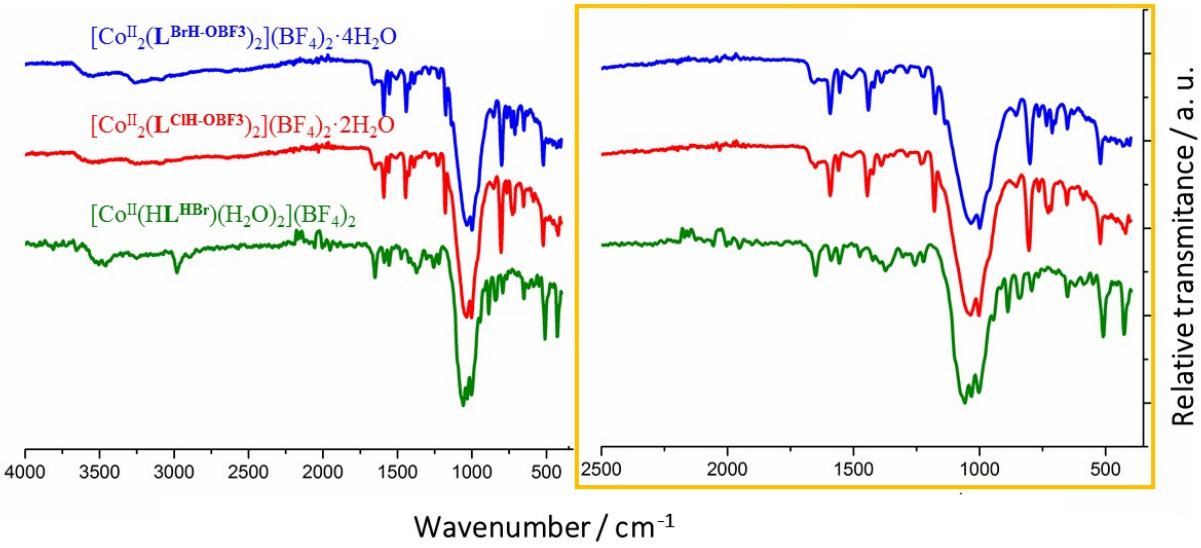

Figure S8. REVISED stacked infrared spectra of compounds **[**Co^{II}_2**(L**$^{BrH-OBF3}$**)**$_2$**]**$(BF_4)_2$·$4H_2O$ (**2'**) (blue), [Co^{II}_2(**L**$^{ClH-OBF3}$)$_2$]$(BF_4)_2$·$2H_2O$ (**3'**) (red) and [Co^{II}(H**L**^{HBr})$(H_2O)_2$]$(BF_4)_2$ **1'** (green). Left: full range 4000-400 cm^{-1}, Right: expansion of 2500-450 cm^{-1}, highlighting the impact on the BF_4 region of the spectrum of the ligand rearrangement seen for two (blue and red spectra) of the three complexes.

Comparison of microanalysis and TGA data matches for various mono- vs di-nuclear formulae for Co(II) BF_4 products of HL^{HR2}

Percentage %	C	H	N
Found	**31.49**	**3.09**	**10.29**
Dinuclear [Co^{II}_2(L$^{ClH-OBF3}$)$_2$](BF$_4$)$_2$·2H$_2$O	31.73 (0.24)	2.66 (0.43)	9.87 (0.42)
TGA	Found 2.96%	Calc. 3.17%	TGA differ: 0.21%
Selection of best fit alternatives (none of which are acceptable)			
Dinuclear [Co^{II}_2(L$^{ClH-OBF3}$)$_2$](BF$_4$)$_2$	32.77 (1.28)	2.38 (0.71)	10.19 (0.10)
Mononuclear [Co^{II}(HL^{ClH})(H$_2$O)$_2$](BF$_4$)$_2$·1MeOH	30.13 (1.36)	3.48 (0.39)	8.78 (1.51)
TGA	Found 2.96%	Calc. 10.10%	TGA differ: **7.14%**
Mononuclear [Co^{II}(HL^{ClH})(MeOH)$_2$](BF$_4$)$_2$	32.21 (0.72)	3.50 (0.41)	8.84 (1.45)
TGA	Found 2.96%	Calc. 9.18%	TGA differ: **6.22%**

Table S1 (CORRECTED). Microanalysis and TGA data for dinuclear **[**Co^{II}_2**(L**$^{ClH-OBF3}$**)**$_2$**]**$(BF_4)_2$·$2H_2O$ (**3'**) showing the difference between found and calculated elemental analysis (Δ) in brackets, for the formulae that were identified to give the lowest Δ (best fits), as well as the difference in found versus calculated TGA results. The best fit to the found values (green boxes) is given in the blue boxes and matches the formulation as a dinuclear complex of rearranged ligand. For comparison, the next best fits (under the orange heading), to both dinuclear complexes of the rearranged and mononuclear complexes of unarranged ligand, none of which are acceptable, are provided in the lower portion of the table.

Percentage %	C	H	N
Found	**27.06**	**2.69**	**8.68**
Dinuclear for $[Co^{II}_2(L^{BrH\text{-}OBF3})_2](BF_4)_2\cdot 4H_2O$	26.70 (0.36)	2.54 (0.15)	8.30 (0.38)
TGA	Found 5.74%	Calc. 5.34%	TGA dffer: 0.40%
Selection of best fit alternatives (none of which are acceptable)			
Dinuclear $[Co^{II}_2(L^{BrH\text{-}OBF3})_2](BF_4)_2$	28.21 (1.15)	2.05 (0.64)	8.77 (0.09)
Mononuclear $[Co^{II}(HL^{BrH})(H_2O)_2](BF_4)_2$	25.93(1.13)	2.61 (0.08)	8.07 (0.61)
TGA	Found 5.74%	Calc. 4.93%	TGA differ: **0.81%**
Mononuclear $[Co^{II}(HL^{BrH})(MeOH)_2](BF_4)_2\cdot 1H_2O$	27.56 (0.50)	3.27 (0.58)	7.56 (1.12)
TGA	Found 5.74%	Calc. 10.20**%**	TGA differ: **4.46%**

Table S2 (CORRECTED). Microanalysis and TGA data for **$[Co^{II}_2(L^{BrH\text{-}OBF3})_2](BF_4)_2\cdot 4H_2O$ (2'**) showing the difference between found and calculated elemental analysis (Δ) in brackets, for the formula that were identified to give the lowest Δ (best fits), as well as the difference in found versus calculated TGA results. The best fit to the found values (green boxes) is given in the blue boxes and matches the formulation as a dinuclear complex of rearranged ligand. For comparison, the next best fits (under the orange heading), to both dinuclear complexes of the rearranged and mononuclear complexes of unarranged ligand, none of which are acceptable, are provided in the lower portion of the table.

FURTHER CORRECTIONS: Please note that Figure S9, and Tables S3 and S4, all of which referred to the impure PF_6 complexes, have been deleted as they were incorrect.

X-ray crystal structure data tables

Table S5. Crystal structure determination details for the complexes $[Co^{II}(HL^{HBr})](MeOH)_2(BF_4)_2$ (**1**), $[Co^{II}_2(L^{BrH\text{-}BF2OMe})]_2(BF_4)_2 \cdot solvents$ (**2**·*solvents*) and $[Co^{II}_2(L^{ClH\text{-}BF2OMe})]_2(BF_4)_2 \cdot solvents$ (**3**·*solvents*).

	1	**2·*solvents*†**	**3·*solvents*†**
Empirical formula	$C_{17}H_{22}B_2Br_2CoF_8N_4O_3$	$C_{32}H_{32}B_4Br_4Co_2F_{12}N_8O_4$	$C_{32}H_{32}B_4Cl_4Co_2F_{12}N_8O_4$
M_r	722.75	1301.39	1123.55
Crystal system	Monoclinic	Monoclinic	Monoclinic
Space group	P 2_1/n	I 2/c	I 2/c
a [Å]	9.6911(4)	15.3342(3)	15.1883(11)
b [Å]	11.6204(4)	17.0365(3)	16.7251(9)
c [Å]	22.6509(7)	20.3884(4)	20.209(2)
α [°]	90	90	90
β [°]	93.838(3)	111.213	110.296
γ [°]	90	90	90
V [Å^3]	2545.09(16)	4965.40(18)	4814.8(7)
Z	4	4	4
T [K]	100	100	100
$\rho_{calcd.}$ [g/cm^3]	1.886	1.741	1.550
μ [mm^{-1}]	9.778	9.799	8.258
F(000)	1420	2536	2248
Crystal Size (mm)	0.341 x 0.118 x 0.090	0.567 x 0.214 x 0.100	0.104 x 0.063 x 0.038
θ range for data collection	3.912 to 74.993°	3.484 to 74.952°	4.076 to 72.241°
Reflections collected	19335	46389	18336
Independent reflections	5129	5076	4831
R(int)	0.0586	0.0820	0.0672
Max. and min. transmission	1.00000 and 0.38435	1.00000 and 0.19241	1.00000 and 0.71629
Data / restraints / parameters	5129 / 9 / 345	5076 / 18 / 298	4831 / 18 / 298
Goof (F^2)	1.045	1.135	1.046
R_1 [I>2σ(I)]	0.0515	0.0738	0.0772
wR_2 [all data]	0.1434	0.1933	0.2278
Max/min res. e density [eÅ^{-3}]	1.291 and -0.881	1.702 and -1.297	0.781 and -0.834

† SQUEEZE applied, see paper for details.

Table S6. Specified hydrogen bonds (with esds except fixed and riding H) for $[Co^{II}(HL^{HBr})(MeOH)_2](BF_4)_2$ **1**.

D-H	H...A	D...A	<(DHA)	
0.84	2.18	2.780(7)	128.5	O1-H1X...F11
0.84	2.09	2.841(6)	148.9	O1-H1X...F12
0.84	2.06	2.781(5)	144.1	O20-H20X...F21
0.84	2.21	2.639(5)	111.4	O30-H30X...O1_$1

Table S7. Selected bond angles (°) for the complexes $[Co^{II}(HL^{HBr})](MeOH)_2(BF_4)_2$ (**1**), $[Co^{II}_2(L^{BrH\text{-}BF2OMe})]_2(BF_4)_2 \cdot solvents$ (**2**·*solvents*) and $[Co^{II}_2(L^{ClH\text{-}BF2OMe})]_2(BF_4)_2 \cdot solvents$ (**3**·*solvents*) at 100 K.

	1	**2·*solvents***	**3·*solvents*†**
N_1-Co-N_2	77.4(1)	74.2(3)	75.0(3)
N_1-Co-N_3	/	112.8(2)	111.6(2)
N_1-Co-N_4	113.2(2)	86.7(2)	85.5(2)
N_1-Co-O_{Me}	/	94.0(3)	92.5(3)
N_1-Co-O_2	87.4(1)	/	/
N_1-Co-O_3	87.5(2)	/	/
N_2-Co-N_3	91.7(2)	/	/
N_2-Co-N_4	/	113.2(3)	112.3(3)
N_2-Co-O_1	/	75.6(3)	75.1(2)
N_2-Co-O_2	90.8(1)	/	/
N_2-Co-O_3	90.4(2)	/	/
N_2-Co- O_{Me}	/	86.3(3)	86.8(3)
N_3-Co-N_4	77.7(2)	76.3(2)	76.7(2)
N_3-Co-O_1	/	100.0(2)	101.0(2)
N_3-Co-O_2	92.4(2)	/	/
N_3-Co-O_3	93.1(2)	/	/
N_3-Co-O_{Me}	/	84.9(3)	85.0(3)
N_4-Co-O_1	/	88.1(2)	88.0(2)
N_4-Co-O_2	89.1(2)	/	/
N_4-Co-O_3	90.7(2)	/	/
O_1-Co-O_{Me}	/	102.4(3)	105.1(2)

† SQUEEZE applied, see paper for details.

Electrochemical studies in MeCN of $[Co^{II}_2(\mathbf{L}^{\mathbf{ClH\text{-}OBF3}})_2](BF_4)_2\cdot 2H_2O$ (**3'**), $[Co^{II}_2(\mathbf{L}^{\mathbf{BrH\text{-}OBF3}})_2](BF_4)_2\cdot 4H_2O$ (**2'**) and $[Co^{II}(H\mathbf{L}^{\mathbf{HBr}})(MeOH)_2](BF_4)_2$ (**1**)

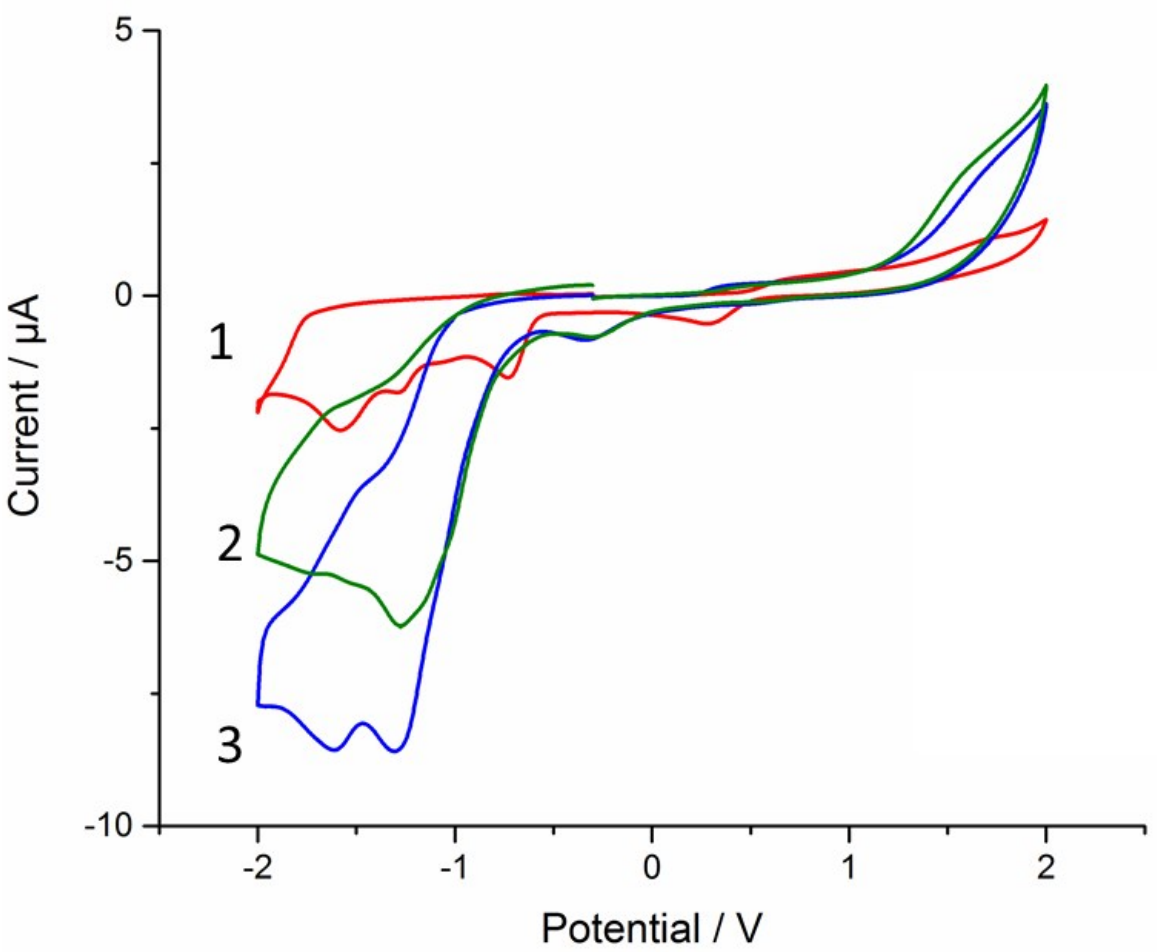

Figure S10. Cyclic voltammograms of $[Co^{II}(H\mathbf{L}^{\mathbf{HBr}})(MeOH)_2](BF_4)_2$ (**1**) (red line), $[Co^{II}_2(\mathbf{L}^{\mathbf{BrH\text{-}OBF3}})_2](BF_4)_2\cdot 4H_2O$ (**2'**) (green line) and $[Co^{II}_2(\mathbf{L}^{\mathbf{ClH\text{-}OBF3}})_2](BF_4)_2\cdot 2H_2O$ (**3'**) (blue line) and as 1 mmol.L^{-1} solutions of cobalt(II) in MeCN (200 mV.s^{-1}, 0.1 mol.L^{-1} NBu_4PF_6, platinum electrode, versus 0.01 mol.L^{-1} $AgNO_3$/Ag).

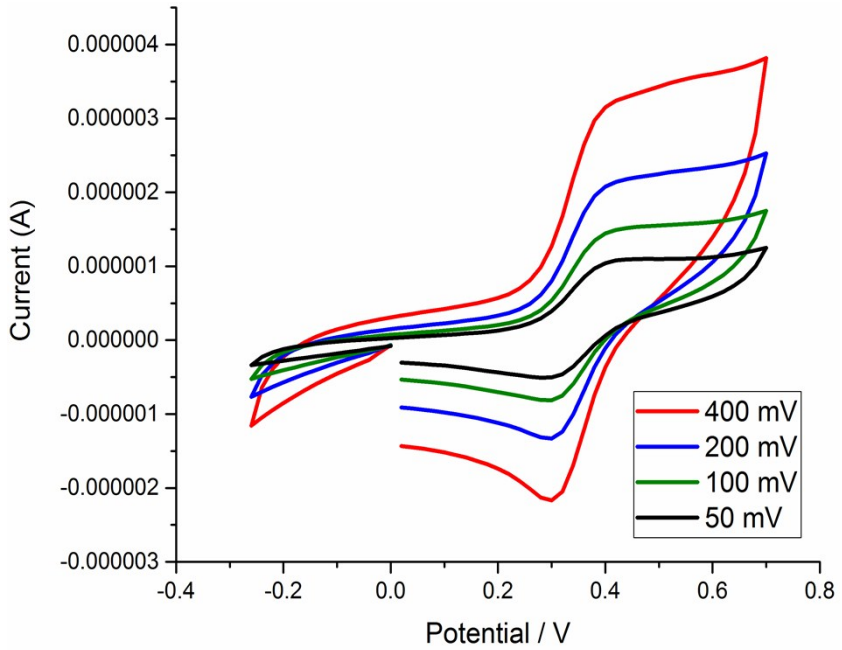

Figure S11. REVISED (scanned to negative potential limit first, but overall very similar to original figure) cyclic voltammograms of $[Co^{II}_2(\mathbf{L}^{\mathbf{BrH\text{-}OBF3}})_2](BF_4)_2 \cdot 4H_2O$ (**2'**) at different scan rates (mVs^{-1}) as 1 mmol L^{-1} solutions in MeCN (0.1 M NBu_4PF_6, platinum electrode, versus 0.01 M $AgNO_3$/Ag).

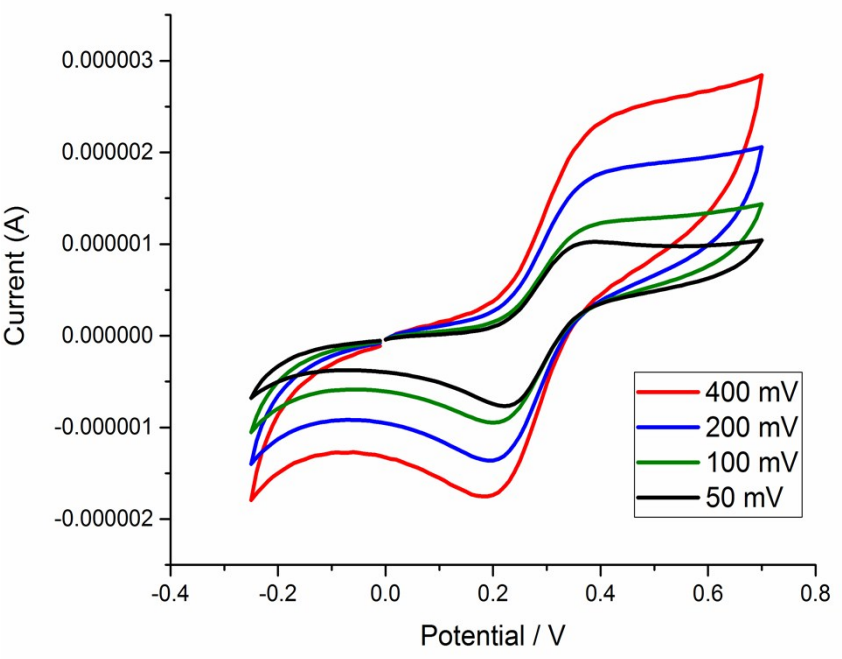

Figure S12. REVISED (but very similar to original figure) cyclic voltammograms of $[Co^{II}_2(\mathbf{L}^{\mathbf{ClH\text{-}OBF3}})_2](BF_4)_2 \cdot 2H_2O$ (**3'**) at different scan rates (mVs^{-1}) as 1mmol L^{-1} solutions in MeCN (0.1 M NBu_4PF_6, platinum electrode, versus 0.01 M $AgNO_3$/Ag).

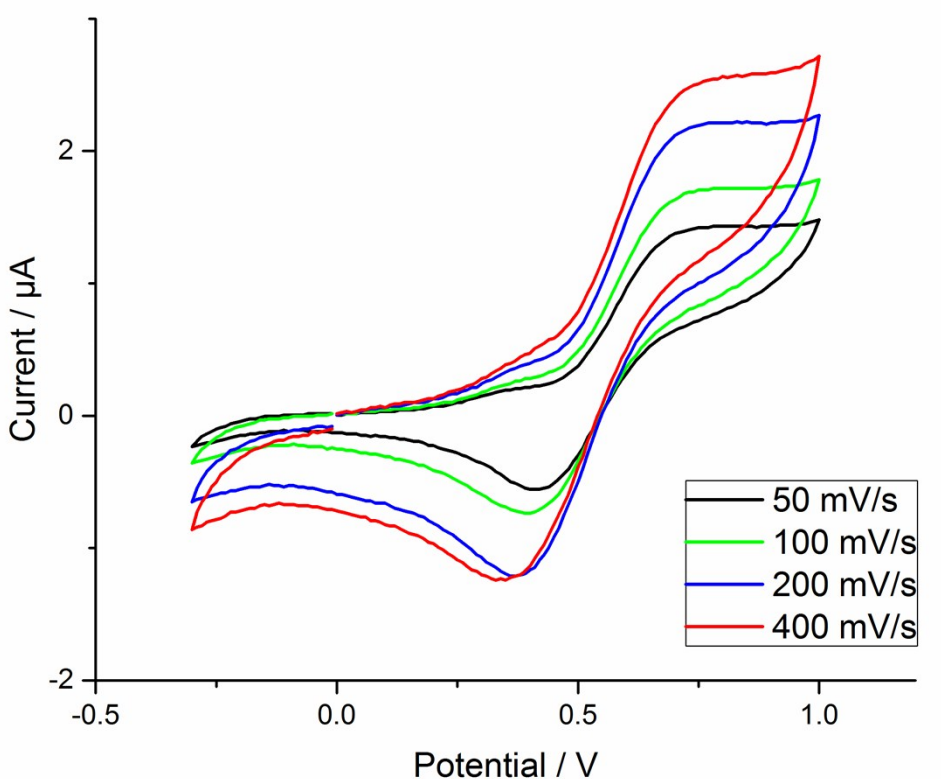

Figure S13. Cyclic voltammograms of $[Co^{II}(HL^{HBr})(MeOH)_2](BF_4)_2$ (**1**) at different scan rates (mVs^{-1}) as 1mmol L^{-1} solutions in MeCN (0.1 M NBu_4PF_6, platinum electrode, versus 0.01 M $AgNO_3$/Ag).

mV/s	Epc	Epa	ΔE	Em
50	0.44	0.30	**0.14**	**0.37**
100	0.44	0.30	**0.14**	**0.37**
200	0.44	0.30	**0.14**	**0.37**
400	0.46	0.30	**0.16**	**0.38**
Average	**0.45**	**0.30**	**0.15**	**0.37**

Table S8. REVISED (but changes are minimal) scan rate study of the process for $[Co^{II}_2(\mathbf{L^{BrH\text{-}OBF3}})_2](BF_4)_2 \cdot 4H_2O$ (**2'**).

mV/s	Epc	Epa	ΔE	Em
50	0.36	0.23	**0.13**	**0.295**
100	0.37	0.22	**0.15**	**0.295**
200	0.38	0.21	**0.17**	**0.295**
400	0.39	0.20	**0.19**	**0.295**
Average	**0.38**	**0.22**	**0.16**	**0.295**

Table S9. REVISED (but changes are minimal) scan rate study of the process for **[**$Co^{II}_2(\mathbf{L^{ClH\text{-}OBF3}})_2](BF_4)_2 \cdot 2H_2O$ (**3'**).

mV/s	Epc	Epa	ΔE	Em
50	0.74	0.40	**0.37**	**0.57**
100	0.75	0.40	**0.37**	**0.57**
200	0.75	0.39	**0.38**	**0.57**
400	0.75	0.37	**0.39**	**0.57**
Average	**0.75**	**0.39**	**0.38**	**0.57**

Table S10. Scan rate study of the process for $[Co^{II}(HL^{HBr})(MeOH)_2](BF_4)_2$ (**1**).

Complex	Em / V	E_{pc} / V	E_{pa} / V	ΔE / V	Ia/Ic
1	0.57	0.75	0.39	0.38	0.75
2'	0.37	0.44	0.30	0.14	0.63
3'	0.29	0.38	0.21	0.17	0.75

Table S11. REVISED (but changes are minimal) summary of electrochemical data obtained by cyclic voltammetry in MeCN at 200 $mV.s^{-1}$ for 1 $mmol.L^{-1}$ of cobalt(II) complexes **1**, **2'** and **3'** (0.1 M NBu_4PF_6, platinum electrode, versus 0.01 M $AgNO_3$/Ag).

References

1. Locke, J.M., et al., *Competition between cyclisation and bisimine formation in the reaction of 1,3-diaminopropanes with aromatic aldehydes.* Tetrahedron, 2009. **65**: p. 10685–10692.